Heritage Science

RESEARCH

Open Access

Application of low-temperature plasma for the removal of copper chloride layers on bronze Wares

Ranran Jiao[1,2], Fuwei Sun[1,2] and Jiaxing Li[1,2,3*]

Abstract

Archaeological objects based on copper alloys (such as bronze wares) usually suffer from "bronze disease" that results from the existence of CuCl on the surfaces. The surface-coating $Cu_2(OH)_3Cl$ can release Cl^- and lead to further corrosion during the storage procedure. The central aim of the work is the verity the effectiveness of low-temperature radio-frequency (RF) plasma for the removal of CuCl and $Cu_2(OH)_3Cl$ from the bronze wares. In this work, CuCl and $Cu_2(OH)_3Cl$ patina were synthesized on copper by a simple solution method. The chemical and aesthetic features before and after plasma treatment were characterized using optical microscopy (OM), SEM-EDS, XRD, and XPS. The results show that Ar-H_2 plasma could reduce the CuCl to Cu efficiently, which achieves pleasing esthetics as well as removes the chlorine (Cl atomic ratio decrease from 46.0 to 3.6%). For $Cu_2(OH)_3Cl$, the air plasma treatment exhibit better performance compared to the Ar-H_2 plasma treatment, judging from the aesthetic effect and the removal effect of chlorine (Cl atomic ratio decrease from 14.8 to 3.3%).

Keywords Copper, Chloride, Low-temperature plasma, Radio frequency

Introduction and research aim

Bronzeware is of vital importance in the river of human civilization, bronze has been used for utensils, decorative and artistic objects since ancient times due to its good corrosion resistance, casting performance, and long-lasting characteristics [1, 2]. Bronze is a composite alloy based on copper with the additions of lead, tin, and other metals [3]. After being buried underground for a long time, their surfaces are usually covered by a cuprous chloride layer (nantokite, CuCl), which is commonly believed to be the main species leading to "bronze disease" [4, 5]. The corresponding reaction can be described as follows,

$$4CuCl + 4H_2O + O_2 \rightarrow 2Cu_2(OH)_3Cl + 2HCl \quad (1)$$

During the reaction, CuCl could react with water to yield $Cu_2(OH)_3Cl$ and HCl [6]. The generated HCl could further corrode the copper alloy, resulting in a chain reaction. Meanwhile, the other corrosion products basic copper chlorides ($CuCl_2{\cdot}3Cu(OH)_2$) are often voluminous, which will destroy the surfaces of bronze wares as well as provide an easy path for the entrance of oxygen and humidity [7]. On the other hand, basic copper chlorides themselves could also release Cl^- and aggravate the corrosion of the copper matrix [8]. Therefore, the removal of chloride species is an efficient method for inhibiting a self-accelerated corrosion process known as "bronze disease" [9].

Traditional methods for the removal of these corrosion layers are mainly composed of the chemical method [10,

*Correspondence:
Jiaxing Li
lijx@ipp.ac.cn
[1] CAS Key Laboratory of Photovoltaic and Energy Conservation Materials, Institute of Plasma Physics, Hefei Institutes of Physical Science, Chinese Academy of Sciences, Hefei 230031, PR China
[2] University of Science and Technology of China, Hefei 230026, Anhui, PR China
[3] Collaborative Innovation Center of Radiation Medicine of Jiangsu Higher Education Institutions, Suzhou, P.R. China

11] and electrochemical methods. Although these methods have been widely used in the past, the removal effects are still far from satisfactory. As a result, many new methods have been developed, that exhibit better performance for the removal of corrosion layers. For example, Wang et al. developed a novel amino acid inhibitor, which will effectively inhibit the hydrolysis reaction of CuCl. The experiment also showed that inhibition efficiency of over 90% can be achieved [12]. Guaragnone and co-authors formulated polyvinyl alcohol (PVA) based highly viscous polymeric dispersions (HVPDs), the confinement of (tetraethylenepentamine) TEPA inside the PVA matrix allowed the progressive removal of copper corrosion products from a 16th -century Italian bronze masterpiece [13].

Low-temperature plasma cleaning involves the removal of corrosion layers and contaminations from surfaces using varieties of energetic plasma such as RF plasma, atmospheric-pressure (AP) plasma jets, dielectric barrier discharge (DBD) plasma, and direct current (DC) glow discharge plasma [14, 15]. Low-temperature plasma initially used for the restoration and conservation of metal artifacts could date back to 1979 [16]. Since then, different plasma (H_2, O_2, Ar, N_2, and so on) [17–20] has been used for the restoration and conservation of metal and other artifacts. Usually, hydrogen gas has been widely employed in plasma treatment based on the fact that most of the corrosion products are metal oxides or chlorides [21, 22]. During this process, the hydrogen species will react with oxygen and chlorine, resulting in the formation of OH radicals and HCl molecules that can be consequently removed from the reaction system [23, 24]. Compared to the traditional methods, the modern plasma chemical treatment is a dry method, which prevents further corrosion caused by water during the treatment [25]. Besides, the contactless and unaggressive working mode could avoid the mechanical shock and local heating of the artifacts, preventing them from further destruction.

Our study aims to evaluate the application of low-temperature RF plasma for the removal of copper chloride layers. In this work, two different corrosion layers (CuCl and $Cu_2(OH)_3Cl$) were prepared, representing the copper with different corrosion extents. The corroded coppers were then treated with plasma (manipulate reaction time and gas composition) to investigate the effectiveness of this method on the removal and turn of chloride layers. The surfaces of corroded copper foil before and after plasma treatment are characterized using optical microscopy, scanning electron microscopy (SEM) with energy dispersive X-ray spectrometer (EDS), and X-ray diffraction (XRD).

Experimental section

Artificial corrosion processes

Morals and laws do not allow experimental cleaning techniques on genuine historical objects. For this reason, the explorations of the experimental cleaning methods have been performed on artificial corroded copper foils.

(1) Firstly, the copper foils were degreased by acetone and ethanol alternatively, and then rinsed with de-ionized water. (2) In the next step, the chemical corrosion processes were performed. For mild corrosion copper sheets (copper sheet covered by CuCl, labeled as MC-copper), the original copper sheets were immersed into the 0.37 mol L^{-1} $CuCl_2$ solution under continuous stirring for 15 min, followed by rinsing with de-ionized water to remove the additional $CuCl_2$. (3) To get serious corrosion copper sheets (copper sheet covered by $Cu_2(OH)_3Cl$, labeled as SC-copper), the first stage specimens were scattered with water and then sealed in a container for 72 h, which led to the formation of green clinoatacamite ($Cu_2(OH)_3Cl$).

Plasma treatment

An inductively coupled plasma device (ICP), which is usually powered by a 13.56 MHz radio frequency (RF) power source, was employed for the surface treatment and the work pressure was evacuated down to 33 Pa (Fig.1). The power of the RF generator is set to 100 W. The reactor is a quartz tube with a size of 5 cm×110 cm (diameter×length). All experiments were carried out at room temperature. Specifically, the selective gas composition and treatment duration are summarized in Table 1. The hydrogen was diluted by argon (ratio in volume%), for one reason, argon minimizes the explosion hazard; for another reason, the metastable states in ionized argon could activate the other gas [26]. The treatments were performed at room temperature. The actual samples' temperatures were tested by a temperature measuring probe, the results show that the temperature is 47℃ after 8 min in Ar/H_2, and 56℃ after 11 min in air. Note that three parallel experiments were executed and the results mean ± standard deviation were obtained.

Analysis and characterization

In this study, optical microscopy was used to study the visual appearances and physical-chemical transformations before and after HF plasma treatment. The optical images were obtained from Leica-microsystems. According to many specialists [7, 22, 27], Thermo Fischer (Helios CX) scanning electron microscope coupled with energy-dispersive X-ray spectroscopy (SEM-EDX) has been used to assess chemical proportions and surface morphology of the samples. The EDS analysis areas are 150 × 90 μm

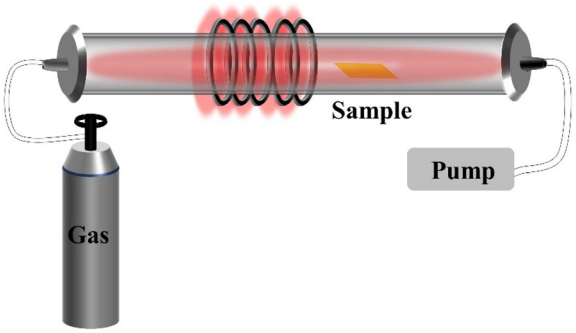

Fig. 1 Scheme of the low-temperature low-pressure RF plasma device

Table 1 Experiment parameters of plasma treatment

Samples	Duration/min	Gas
MC-copper-3	3	Ar-10%H_2
MC-copper-5	5	Ar-10%H_2
MC-copper-8	8	Ar-10%H_2
SC-copper-5	5	Ar-10%H_2
SC-copper-8	8	Ar-10%H_2
SC-copper-11	11	Ar-10%H_2
SC-copper-3*	3	Air
SC-copper-5*	5	Air
SC-copper-8*	8	Air

MC-copper-x: mild corrosion copper sheets, copper sheet covered by CuCl; SC-copper-x: serious corrosion copper sheets, copper sheet covered by $Cu_2(OH)_3Cl$; x means time, min.

Asterisk means in the air

in these experiments. The crystalline phases of the corrosion sheet sample (copper foil covered by corrosion layer) were determined by X-ray diffraction (XRD Rigaku Smartlab 9) with Cu Kα radiation (λ = 1.5406 Å) and the assignment of phases was based on the JPDS powder diffraction cards [24]. According to many specialists, X-ray photoelectron spectra (XPS) of the samples were determined using an ESCALAB 250 + instrument (Thermo Fischer, EACALAB 250Xi) to obtain the valence, and calibration was carried out by C1s peak (binding energy = 284.8 eV) [12, 28, 29]. The XPS analysis areas is a circular area with diameter of 400 μm. To measure the inner states, the surface was etched in the preparation chamber of the XPS instrument by Ar + ions beamline (2 keV), 2 min per cycle.

Results and discussion

Hydrogen plasma treatment of CuCl

Although chemicals with complex constituents, such as nantokite (CuCl), romarkite (SnO), cassiterite (SnO_2), cuprite (Cu_2O), tenorite (CuO), malachite [$Cu_2(OH)_2CO_3$], cerussite ($PbCO_3$), piromorfite [(PbCl) $Pb_4(PO_4)_3$], smithsonite ($ZnCO_3$) and so on, have been found in patina [9, 30, 31], the previous studies have indicated that the most aggressive corrosion agent for Cu-based artifacts is chlorine (Cl^-). The first stage of Cl^- based corrosion is the formation of cuprous chloride (nantokite, CuCl). And that is why we prepared artificially corroded CuCl model samples by chemical treatment.

As it is shown in Fig. 2a, MC-copper was covered with uniform thin grey corrosion layers compared to raw copper after the first stage of the chemically induced corrosion in $CuCl_2$ solution (Fig. 2b). The SEM images indicate the rough surfaces after the first stage of chemical etching in the $CuCl_2$ (Fig. 2c). It can be seen that the as-formed patina is composed of multi-angular particles and numerous small particles. The XRD patterns of the raw copper and artificially corroded samples are shown in Fig. 2d, which indicates the formation of CuCl after chemical treatment. The blue line in Fig. 2d can be indexed to the cubic phased CuCl (PDF#04-007-3879) and Cu base, suggesting the formation of CuCl. The EDS analysis suggests that the corrosion layer consists of Cu and Cl (Fig. 2e), which agrees well with the XRD result. The atomic ratio between Cu and Cl is approximately 1:1 (Cu 54.0 ± 0.42%, Cl 46.0 ± 0.42%), which is consistent

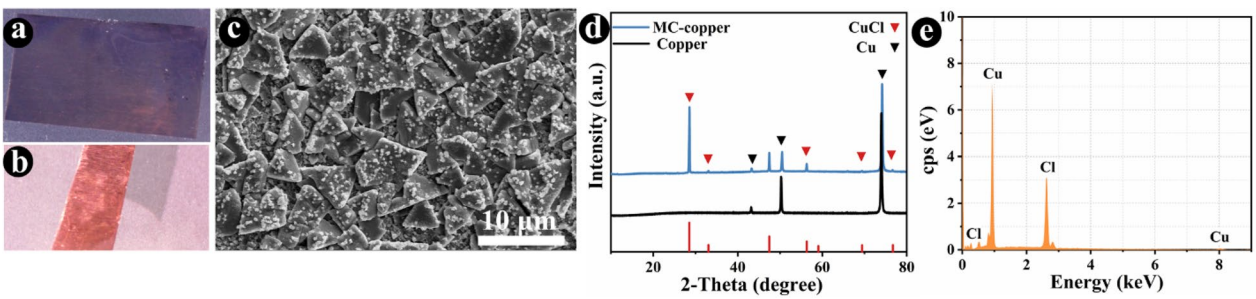

Fig. 2 Photographic images after **a** and before **b** the immersion in $CuCl_2$ solution. SEM **c** XRD **d** and EDS **e** after the immersion in $CuCl_2$ solution

with the theoretical value of CuCl. Taking the above analysis and △G values into consideration, the reaction equation can be described as follows:

$$Cu + CuCl_2(aq) \rightarrow 2CuCl\ (s) \quad (2)$$

The samples were treated at different time at room temperature by hydrogen glow discharge plasma technique, keeping the output power and pressure constant (100 W, 33 Pa). Room temperature conditions avoid grain growth or recrystallization of the metallic objects. The effect of plasma reduction is evident even the treating time is as short as 3 min. The surface of the copper turns shiny red, indicating the reduction of CuCl to Cu (Fig. 3a). While prolonging the treatment time, the surface of the copper became more and more bright (Fig. 3b and c). However, the original gloss cannot be regained (the same as Fig. 2b), which is mainly caused by the increase in surface roughness during the process of corrosion. EDS examinations of the three samples also proved the effectiveness of this method (Fig. 3d–f), the atomic concentration of Cl decreases after plasma treatment down to 4.5%-3.6% depending on the

Table 2 Atomic concentration (%) of MC-copper after hydrogen plasma treatment through EDS bulk analysis

Sample	Atomic percentages (%)	
	Cu / total metals	Cl / total metals
MC-copper-3 (CuCl, 3 min)	95.4 ± 0.74	**4.5** ± 0.74
MC-copper-5 (CuCl, 5 min)	95.3 ± 2.53	**4.6** ± 2.5
MC-copper-8 (CuCl, 8 min)	96.4 ± 1.5	**3.6** ± 1.46

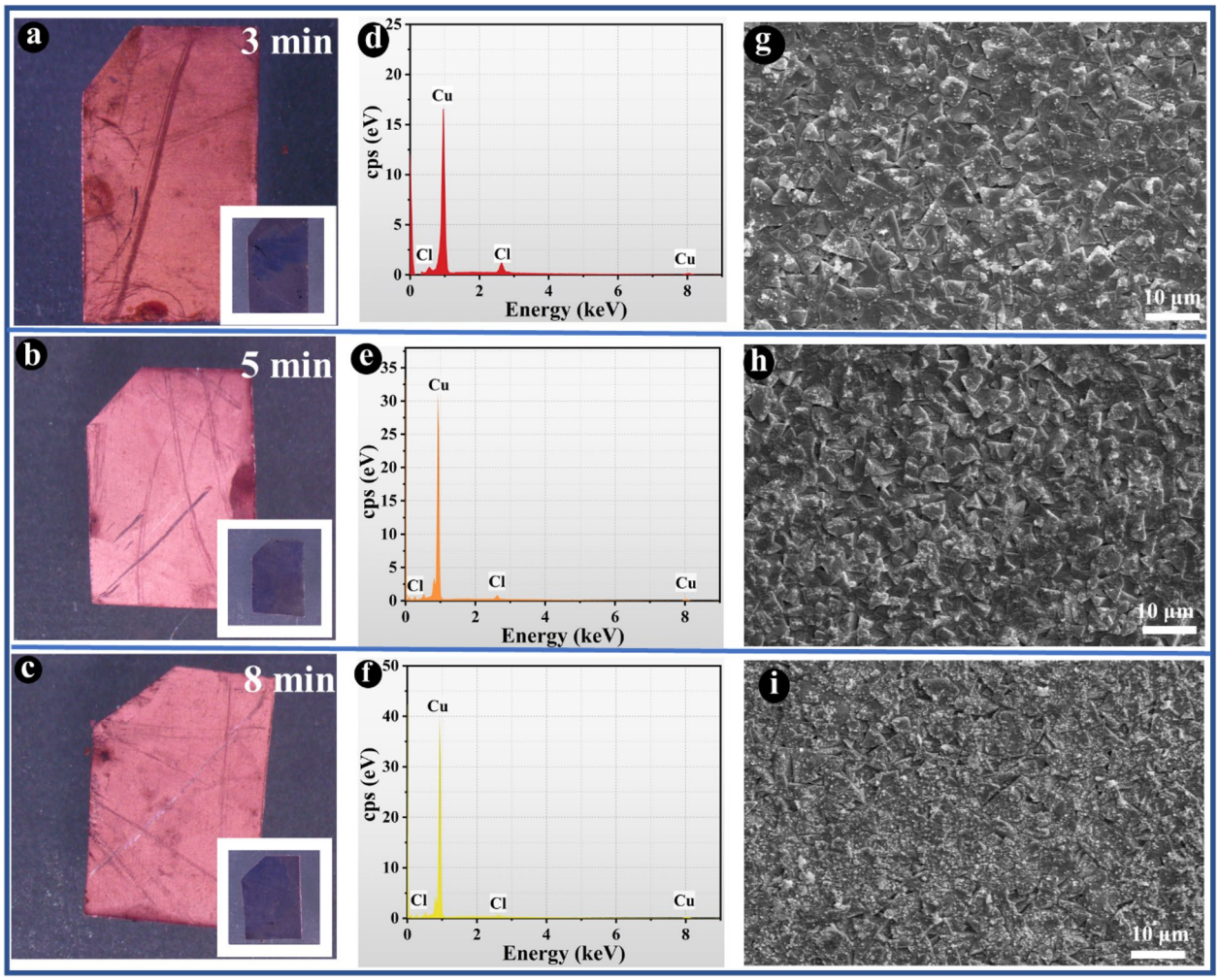

Fig. 3 MC-copper-3: photographic images **a**, EDS **d** and SEM **g**; MC-copper-5: photographic images **b**, EDS **e** and SEM **h**; MC-copper-8: photographic images **c**, EDS **f** and SEM **i**

treatment conditions (Table 2). As shown in Fig. 3 g–i, the surface of the samples after the plasma treatment shows similar morphology to raw CuCl-covered copper, but smaller particles due to the effect of plasma treatment.

To further explore the valence states of Cu before and after treatment, XPS analyses were performed (Fig. 4). The peaks of Cu 2p, O 1s, C 1s, and Cl 2p can be observed, in which the signals of C and O come from the atmosphere contamination (Fig. 4a). The deconvoluted profiles of Cu 2p suggested the presence Cu^0, Cu^+, and Cu^{2+} in the MC-copper sample (Fig. 4b), in which the Cu^{2+} can be attributed to the oxidation of CuCl because of the instability of CuCl [32, 33]. Figure 4c shows the spectra of Cu 2p after different treatment times. The two peaks centering at 952.5 eV and 932.7 eV can be attributed to Cu 2p3/2 and Cu 2p1/2 components, respectively, with split spin-orbit components of 19.8 eV [34, 35]. No satellite between the two peaks is observed, which is a typical spectrum characteristic of metallic Cu. These results demonstrate that the hydrogen plasma can efficiently eliminate the CuCl corrosion layer and even completely reduces it back to copper.

Plasma treatment of $Cu_2(OH)_3Cl$

When CuCl contacts with moisture, a dangerous cyclical phenomenon called bronze disease will occur by forming clinoatacamite and its polymorphs ($Cu_2(OH)_3Cl$) [36, 37]. For this reason, we simulated the further corrosion process of CuCl. SC-copper will be obtained after further corrosion in moist air, which is covered with a similar patina consisting of a uniform smooth white layer with green and yellowish areas (Fig. 5a). This phenomenon reveals the occurrence of "bronze disease" and active corrosion. The characterization results of SEM, XRD, and EDS for the artificial patina are shown in Fig. 5b–d. The SEM image of the sample clearly demonstrates that the as-formed $Cu_2(OH)_3Cl$ patina are lumps with sizes of ~3 μm, which is totally different from CuCl patina. XRD patterns together with the EDS of the SC-copper disclose the same chemical composition as Mc-copper. The green layer consists mainly of basic copper chlorides

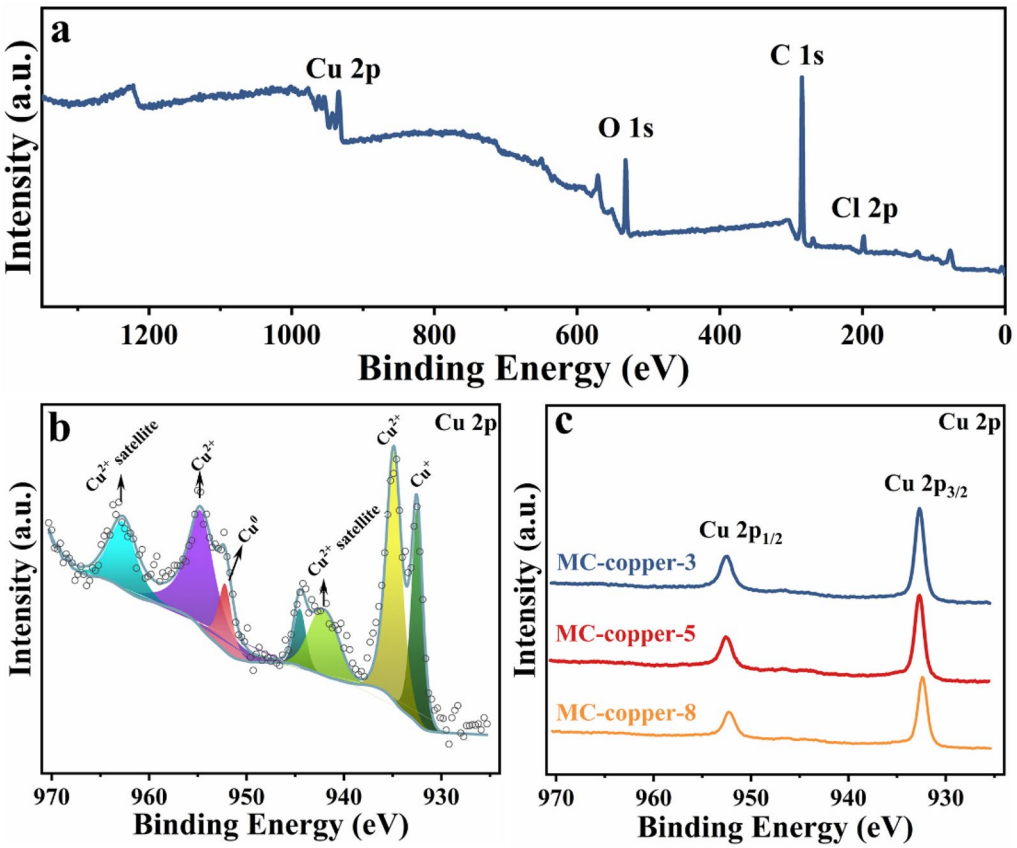

Fig. 4 The XPS survey **a** and deconvoluted profiles of Cu 2p **b** of MC-copper; The high resolution of Cu 2p spectra for different treatment conditions **c**

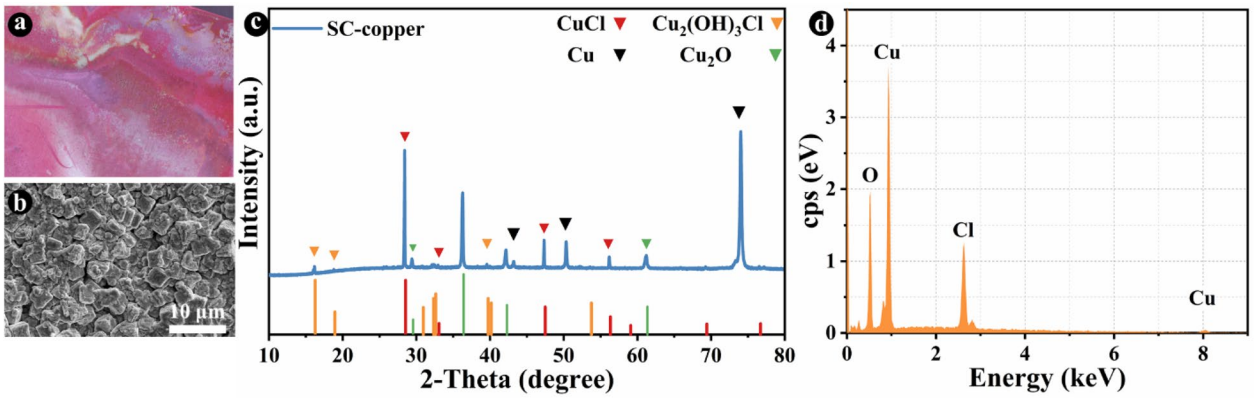

Fig. 5 Photographic images **a**, SEM **b** XRD **c** and EDS **d** of SC-copper

(Clinoatacamite, $Cu_2(OH)_3Cl$, PDF#99-000-0752), while the red layers of cuprite (Cu_2O, PDF#97-017-3982). The results clearly indicate that surface corrosion possesses the same chemical composition as the bronze disease. Being calculated from the EDS analysis, the Cl atomic percentage in the patina is 14.8 ± 3.8% (Cu 42.3 ± 6.8%, O 42.8 ± 3.3%).

For the plasma treatment of the SC-copper, gases with reductive characteristics (hydrogen) and their diluted mixtures with argon were used. From a visual inspection of the cleaned SC-copper (Fig. 6a–c), the metal regions which were not covered by green areas recovered to their original metal surface. The green areas (mainly composed of $Cu_2(OH)_3Cl$) turn into black CuO. Even after prolonging the treatment time to 11 min, the black CuO cannot be reduced to Cu, suggesting that the cleaning efficiency of $Cu_2(OH)_3Cl$ is lower than CuCl. Still and all, the aim of chloride removal was achieved according to the EDS results. The EDS result reveals a remarkable decrease in the chloride content by the intensity of the Cl peak in Fig. 6d–f and quantitative analysis of Cl (Table 3). The removal efficiency is proportional to the duration of the plasma treatment. Moreover, as the treatment time increases, a rougher surface appears (Fig. 6g–i), which is inevitable because of the etching effect of the plasma.

Moreover, XPS investigation was also employed to investigate the changes in valence states in SC-copper before and after plasma treatment. As is shown in Fig. 6j, the XPS results of raw SC-copper clearly show peaks of the native basic copper chlorides and Cu base. After plasma treatment in the H_2 atmosphere (SC-copper-5, SC-copper-8, and SC-copper-11 in Fig. 6j), only the main peaks of Cu 2p3/2 positioned at 932.5 eV and Cu 2p1/2 positioned at 952.3 eV remain, suggesting the successful reduction of basic copper chlorides. The deconvoluted profiles of SC-copper-11 are shown in Fig. 6j, the weak Cu^{2+} peaks, and its satellite peaks can be attributed to the black CuO layers.

The above results clearly suggest that hydrogen plasma treatment could turn basic copper chlorides into CuO according to Eq. 3, during which Cl can be totally removed. The gradual elimination of the chlorine-containing corrosion products could result in the formation of more stable species such as black CuO. However, an indisputable flaw is that the original color of samples changes as the formation of CuO and removal of Cl.

$$Cu_2(OH)_3Cl \rightarrow CuO + HCl \quad (3)$$

Based on the above results, we also used the gases with oxidant characteristics (air plasma) for treating the SC-copper. The results are shown in Fig. 7. After 3 min treatment (Fig. 7a and b), the thin green layer turned into dark brown and the Cl content slightly decreased to ~ 10.2% (Table 4). By prolonging the treatment time, the areas of $Cu_2(OH)_3Cl$ became darker and the content of Cl decreased (Fig. 7c–f). After 8 min treatment, the atomic concentration of Cl decreases to 3.3%. As expected, the high-resolution atlas of Cu2p in the three samples is typically Cu(II) in Cu(II) oxides [38–41]. Considering several factors, including the aesthetic effect, the removal effect of chlorine, and cost, air plasma remains more satisfactory than hydrogen plasma.

Plasma cleaning is a surface treatment technology, a corrosion layer usually still exists even after the plasma treatment [22, 28]. To figure out the depth penetration of the treatment, the cross-sectional SEM image and EDS linear scan of Cl were carried out. For sample MC-copper-8 (Fig. 8a), the SEM observation of the cross-section reveals that the thickness of corrosion layer is about 7.5 μm, with an obvious boundary between Cu base and

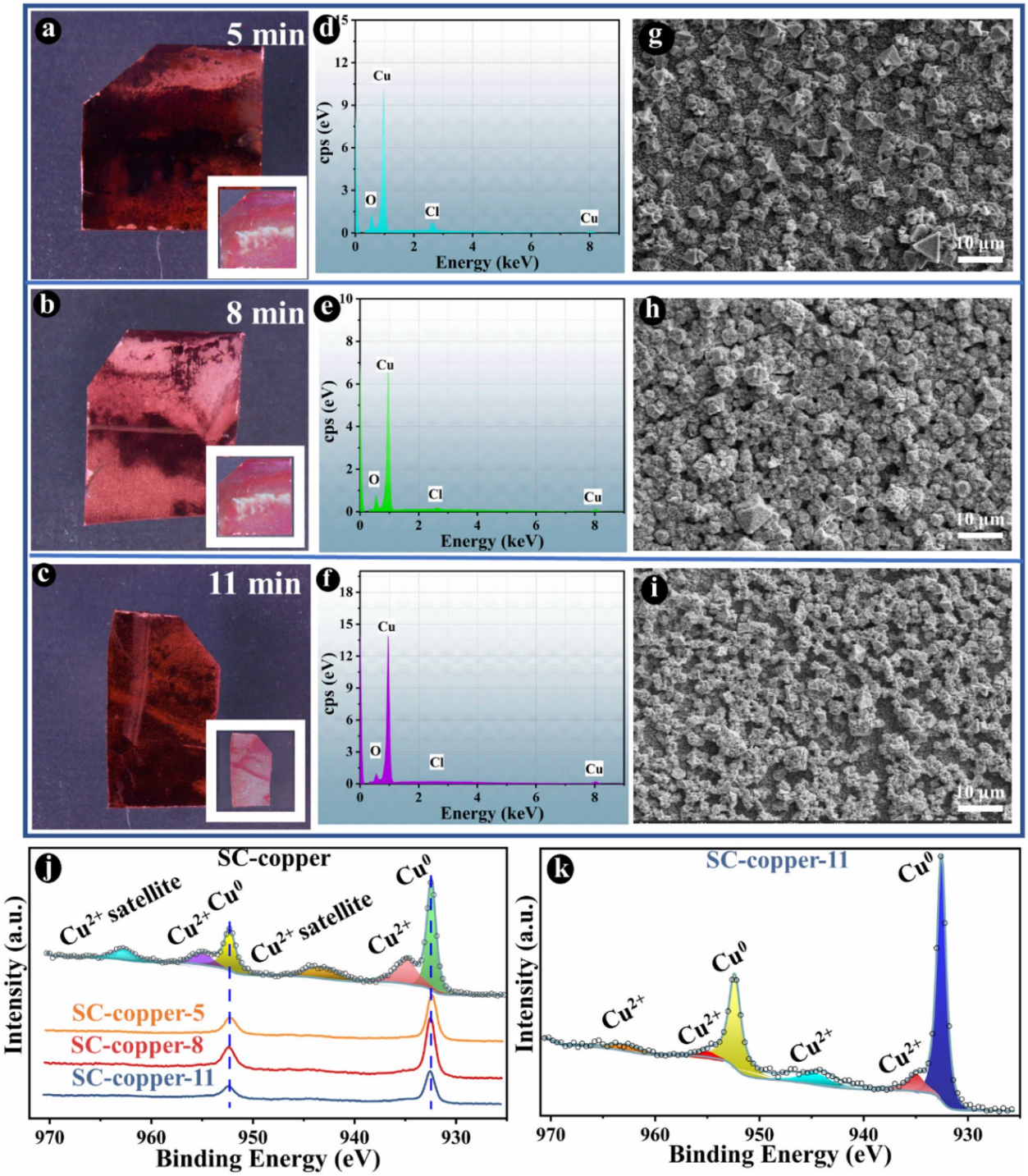

Fig. 6 SC-copper-5: photographic images **a**, EDS **d** and SEM **g**; SC-copper-8: photographic images **b**, EDS **e** and SEM **h**; SC-copper-11: photographic images **c**, EDS **f** and SEM **i**; **j**: Deconvoluted profiles of Cu 2p of SC-copper and high resolution of SC-copper-5, SC-copper-8 and SC-copper-11; **k** Deconvoluted profiles of Cu 2p of SC-copper-11

corrosion layer. Additionally, the EDS linear scan of the cross section clearly shows the elemental distribution of Cl after plasma treatment as a function of the corrosion thickness (Fig. 8a). In Fig. 8a section I (about 3 μm in thickness), the Cl is almost totally removed, demonstrating the effectiveness of Ar/H_2 plasma cleaning process.

Table 3 Atomic concentration (%) of SC-copper after hydrogen plasma treatment through EDS bulk analysis

Sample	Atomic percentages (%)		
	Cu/total metals	Cl/total metals	O/total metals
SC-copper-5 ($Cu_2(OH)_3Cl$, 5 min)	61.0 ± 5.9	**7.9** ± 1.6	31.1 ± 5.5
SC-copper-8 ($Cu_2(OH)_3Cl$, 8 min)	70.7 ± 7.6	**4.3** ± 1.7	24.9 ± 7.2
SC-copper-11 ($Cu_2(OH)_3Cl$, 11 min)	74.9 ± 9.5	**3.0** ± 2.1	22.0 ± 7.4

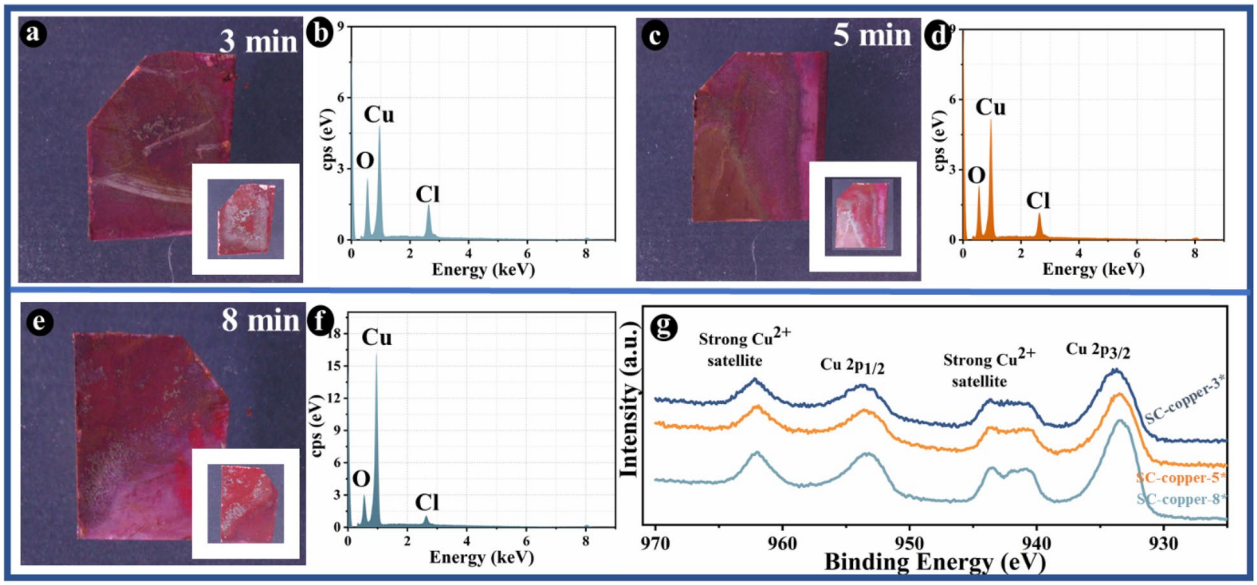

Fig. 7 SC-copper-3*: photographic images **a** and EDS **b**; SC-copper-5*: photographic images **c** and EDS **d**; SC-copper-8*: photographic images **e** and EDS **f**; **g** The high resolution of Cu 2p spectra for SC-copper-3*, SC-copper-5* and SC-copper-8*

Table 4 Atomic concentration (%) of SC-copper after air plasma treatment through EDS bulk analysis

Sample	Atomic percentages (%)		
	Cu/total metals	Cl/total metals	O/total metals
SC-copper-3* ($Cu_2(OH)_3Cl$, 3 min)	43.0 ± 6.3	**10.2** ± 4.6	46.7 ± 2.0
SC-copper-5* ($Cu_2(OH)_3Cl$, 5 min)	40.7 ± 1.1	**11.1** ± 1.5	48.2 ± 1.3
SC-copper-8* ($Cu_2(OH)_3Cl$, 8 min)	54.6 ± 6.1	**3.3** ± 1.7	42.0 ± 7.8

Asterisk means in the air

As the depth further increases, the concentration of Cl increases evidently (section II in Fig. 8a) because of the insufficient penetration depth of the plasma technology. For sample SC-copper-8* (Fig. 8b), the thickness of corrosion layer is 12–19 μm, which is much larger than sample MC-copper. The elemental distribution of Cl can be divided into four sections after the air plasma treatment. In Fig. 8b section I, the Cl is almost totally removed (about 4.5 μm in thickness). In Fig. 8b section II, the concentration of Cl gradually increases. However, the concentration of Cl is still lower than the corresponding values in sample MC-copper-8, suggesting a higher efficiency. This phenomenon may be associated with the pores and cracks in the corrosion layer which can make plasma cleaning process more efficient. Unsurprisingly, in Fig. 8b section III has the highest Cl residue because of the limited penetration depth of plasma.

To further investigate the elemental distribution of Cl, a high-resolution narrow spectrum of Cl 2p after the sputtering procedure was recorded. For sample

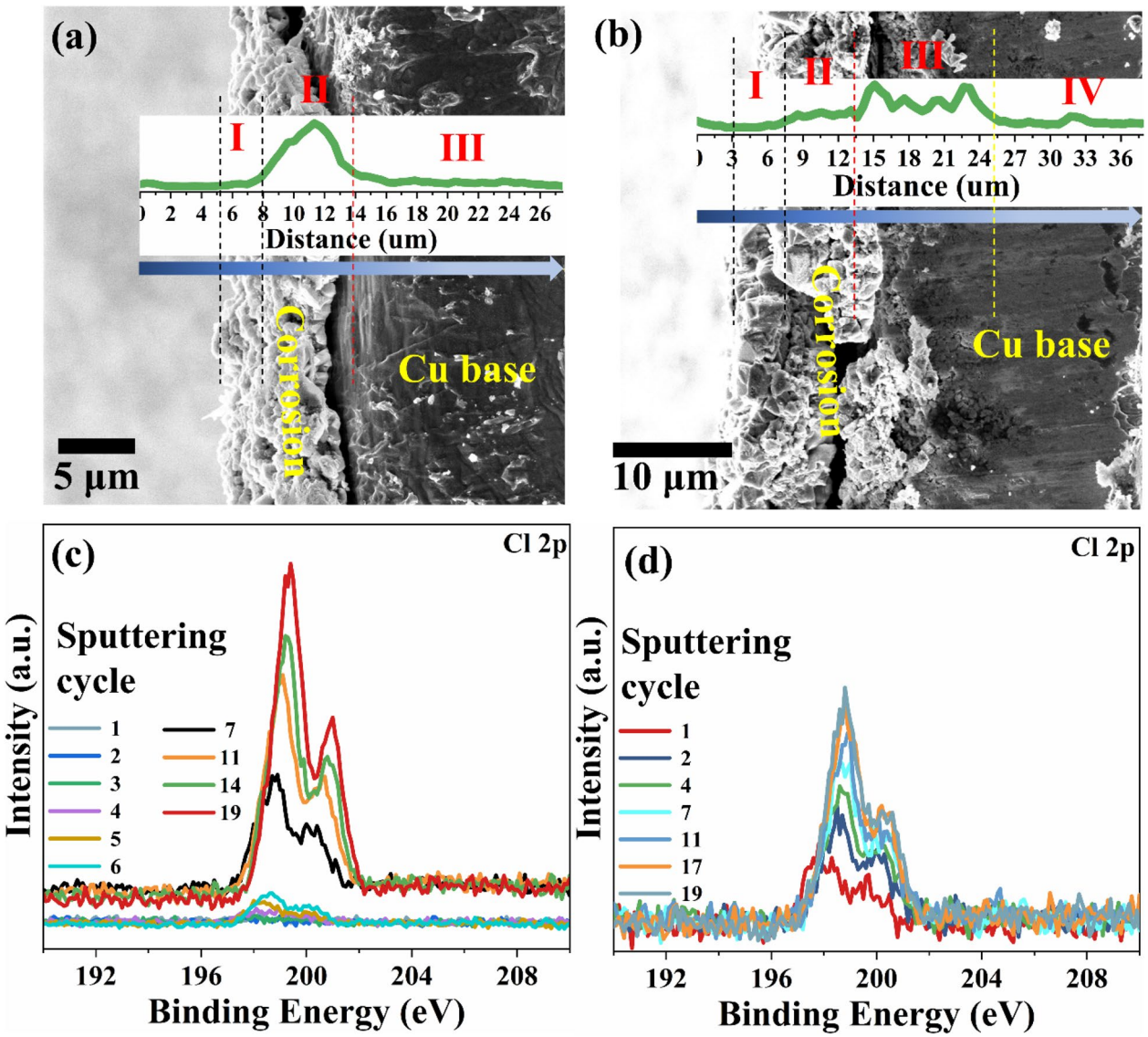

Fig. 8 MC-copper-8: the cross-sectional SEM image and EDS linear scan **a**, high resolution XPS spectra after different subsequent sputtering cycles **c**; SC-copper-8*: the cross-sectional SEM image and EDS linear scan **b**, high resolution XPS spectra after different subsequent sputtering cycles **d**

MC-copper-8 (Fig. 8c), there is no obvious Cl peak in the first 6 cycles. While the intensity of Cl peak increases with the etching depth from 7th to 19th cycles, which is consistent with linear scan result of the cross-section. For sample SC-copper-8*, the intensity of Cl peak is larger than the corresponding value in sample MC-copper-8 in the first cycles, which means that more Cl remnant in SC-copper-8*. Moreover, the same to the MC-copper-8, the intensity of Cl peak increase with the etching depth.

Conclusion

This work studied the effect of plasma on different chlorides that are the root of "bronze disease", described the chemical composition after plasma treatment, and evaluated the results according to the conservation requirements. Generally, Ar-H_2 plasma could reduce the CuCl to Cu efficiently, which achieves pleasing esthetics as well as removes chlorine (about 3.6% Cl residual). However, the effect of Ar-H_2 plasma on $Cu_{2(}OH)_3Cl$ is unsatisfactory due to the formation of a black layer though only

about 3.0% Cl residual, while air plasma could oxidize the $Cu_2(OH)_3Cl$ patina to dark brown CuO and remove chlorine (about 3.3% Cl residual).

Note that the plasma technique could be considered a good treatment for mildly corroded archaeological bronze objects due to its qualities. For warty corrosion, plasma pretreatment ally with additional treatment such as chemical treatment should be considered.

Abbreviations

RF	radio frequency
OM	optical microscopy
PVA	polyvinyl alcohol
HVPDs	polymeric dispersions
TEPA	tetraethylenepentamine
AP	atmospheric-pressure
DBD	dielectric-barrier discharge
DC	direct current
SEM	scanning electron microscopy
EDS	energy dispersive X-ray spectrometer
XRD	X-ray diffraction
XPS	X-ray photoelectron spectra.

Acknowledgements
Not applicable.

Author contributions
RJ wrote the manuscript, FS and JL reviewed the entire text. All authors read and approved the final manuscript.

Funding
The authors acknowledge the financial support provided by National Key Research and Development Project (2020YFC1522004).

Availability of data and materials
All data generated or analyzed during this study are included in this published article.

Declarations

Competing interests
The authors declare that they have no competing interests.

Received: 17 September 2022 Accepted: 28 November 2022
Published online: 09 February 2023

References

1. Mikić D, Otmačić Ćurković H, Kosec T, Peko N. An Electrochemical and Spectroscopic Study of Surfaces on bronze sculptures exposed to Urban Environment. Materials. 2021. https://doi.org/10.3390/ma14082063.
2. Mason A, Powell W, Bankoff HA, Mathur R, Price M, Bulatović A, Filipović V. Provenance of Tin in the late bronze age Balkans based on probabilistic and spatial analysis of Sn Isotopes. J Archaeol Sci. 2020;122.
3. Liang Z, Jiang K, Zhang T-a. Corrosion behaviour of lead bronze from the western Zhou Dynasty in an Archaeological-Soil Medium. Corros Sci. 2021;191.
4. Hu Y, Wei Y, Li L, Zhang J, Chen J, Same Site. Different corrosion Phenomena caused by Chloride: the Effect of the Archaeological Context on Bronzes from Sujialong Cemetery, China. J Cult Herit. 2021;52:23–30.
5. Grayburn R, Dowsett M, Hand M, Sabbe P-J, Thompson P, Adriaens A. Tracking the progression of bronze disease – a Synchrotron X-Ray Diffraction Study of Nantokite Hydrolysis. Corros Sci. 2015;91:220–3.
6. Bernabale M, Nigro L, Montanari D, De Vito C. Exploring the Chemical composition and corrosion patterns of arrowheads used in the siege of Motya (397 bc) through a Multi-Analytical Approach. J Cult Herit. 2021;52:146–52.
7. Novakovic J, Papadopoulou O, Vassiliou P, Filippaki E, Bassiakos Y. Plasma reduction of bronze corrosion developed under long-term Artificial Ageing. Anal Bioanal Chem. 2009;395:2235–44.
8. Ding K, Qu R, Zhou L, Zhang D, Chen J, He X, Wang L, Wang H, Dou H. In situ Preparation of Cucl cubic particles on the commercial copper foil: its significant facilitation to the Electrochemical performance of the Commercial Graphite and its unexpected photochromic behavior. J Alloys Compd. 2020;835:155302.
9. Faraldi F, Angelini E, Riccucci C, Mezzi A, Caschera D, Grassini S. Innovative Diamond-Like Carbon Coatings for the conservation of Bronzes. Surf Interface Anal. 2014;46:764–70.
10. Normand-Chave C, Leprince P. Dussère F. plasma treatment of Artefacts. Surf Eng. 2013;17:236–40.
11. Grassini S, Angelini E, Mao Y, Novakovic J, Vassiliou P. Aesthetic Coatings for Silver Based Alloys with Improved Protection Efficiency. Prog Org Coat. 2011;72:131–7.
12. Wang T, Wang J, Wu Y. The inhibition effect and mechanism of L-Cysteine on the corrosion of bronze covered with a Cucl Patina. Corros Sci. 2015;97:89–99.
13. Guaragnone T, Casini A, Chelazzi D, Giorgi R. Pva-based Peelable Films loaded with tetraethylenepentamine for the removal of Corrosion products from bronze. Appl Mater Today. 2020;19.
14. El-Gohary, MA, METAWA A. Cleaning of architectural Bricks using rf plasma. I. Metallic Stains. Int J Conserv Sci. 2016;7:669–82.
15. Török T, Urbán P,LassúG. Surface cleaning and Corrosion Protection using plasma technology. Int J Corros Scale Inhib. 2015;4:116–24.
16. Daniels VD, Holland L, Pascoe MW. Gas plasma reactions for the conservation of antiquities. Stud Conserv. 1979;24:85–92.
17. Ioanid EG, Rusu DE, Vlad AM, Dunca S, Tanase C, Frunza V, Savin G. Ursescu MC. Multipurpose equipment for radio frequency plasma decontamination and protective coating of Paper materials. IEEE T Plasma Sci. 2016;44:3037–41.
18. Geweely NS. A novel comparative review between Chemical, Natural essential oils and physical (ozone) conservation of Archaeological Objects against Microbial Deterioration. Geomicrobiol J. 2022;39:531–40.
19. Vizárová K, Kaliňáková B, Tiňo R. Vajová I,Čížová K. Microbial Decontamination of Lignocellulosic materials with low-temperature Atmospheric plasma. J Cult Herit. 2021;47:28–33.
20. Stefanova M, Kamenarov Z, Sassoni E, Franzoni E, Ripà M, Patelli A, Sakaj M, Scopece P, Verga Falzacappa E. Innovative solutions for prehistoric paintings - Atmospheric pressure plasma and phosphate consolidant for the preservation of the Magura Cave (Bulgaria). IOP Conf Ser: Mater Sci Eng. 2020;949.
21. Sazavska V, Balastikova R, Krcma F, Radkova L, Fojtikova P, Prikryl R. Prochazka M. Plasmachemical Conservation of Corroded metallic objects. J Phys: Conf Ser. 2016;715:012012.
22. Schalm O, Storme P, Gambirasi A, Favaro M, Patelli A. How effective are reducing plasma afterglows at Atmospheric pressure in removing Sulphide Layers: application on tarnished silver, Sterling Silver and Copper. Surf Interface Anal. 2018;50:32–42.
23. Abdel-Maksoud G, Awad H, Rashed U. Different cleaning techniques for removal of Iron Stain from Archaeological Bone Artifacts: a review. Egypt J Chem. 2021;65:69–83.
24. Krčma F, et al. Application of low temperature plasmas for Restoration/Conservation of Archaeological Objects. J Phys: Conf Ser. 2014;565:012012.
25. Pradhan SK, Jeevitha M, Singh SK. Plasma cleaning of Old Indian Coin in H_2–Ar Atmosphere. Appl Surf Sci. 2015;357:445–51.
26. Daniels VD, Holland L, Pascoe MW. Gas plasma reactions for the for the conservation of antiquities. Stud Conserv. 1979;24:85–92.
27. Ioanid EG, Ioanid A, Rusu DE, Popescu C-M, Stoica I. Surface changes upon high-frequency plasma treatment of Heritage photographs. J Cult Herit. 2011;12:399–407.
28. Schalm O, Patelli A, Storme P, Crabbé A, Voltolina S, Feyer V, Terryn H. Tarnished silver–copper surfaces reduction using Remote Helium

plasma at Atmospheric pressure studied by means of high-resolution Synchrotron X-Ray Photoelectron Microscopy. Corros Sci. 2021;178.
29. Favre-Quattropani L, Groening P, Ramseyer D, Schlapbach L. The Protection of Metallic Archaeological Objects using plasma polymer Coatings. Surf Coat Technol. 2000;125:377–82.
30. Casaletto MP, De Caro T, Ingo GM, Riccucci C. Production of reference "Ancient" Cu-Based alloys and their accelerated degradation methods. Appl Phys A. 2006;83:617–22.
31. Graaf MJd, Severens RJ, IJzendoorn LJv, Munnik F, Meijers HJM, Kars H. Sanden MCMvd,Schram DC. Cleaning of Iron Archaeological Artefacts by Cascaded Arc plasma treatment. Surf Coat Technol. 1995;74–75:351–4.
32. Huang Y, Tao Y, He L, Duan Y, Xiao J, Li Z. Preparation of Cucl@Ac with High Co Adsorption Capacity and Selectivity from Co/N_2 binary mixture. Adsorption. 2015;21:373–81.
33. Yang R, Lu X, Huang X, Chen Z, Zhang X, Xu M, Song Q. Zhu L. Bi-Component Cu_2o–Cucl composites with tunable oxygen vacancies and enhanced Photocatalytic Properties. Appl Catal B: Environ. 2015;170–171:225–32.
34. Appa Rao BV, Yakub Iqbal M, Sreedhar B. Self-assembled monolayer of 2-(Octadecylthio)Benzothiazole for Corrosion Protection of copper. Corros Sci. 2009;51:1441–52.
35. Ghahremaninezhad A, Dixon DG, Asselin E. Electrochemical and Xps Analysis of Chalcopyrite ($Cufes_2$) dissolution in Sulfuric Acid Solution. Electrochim Acta. 2013;87:97–112.
36. Tang Y, Cai L, Wang Y, Wang M, Zhou H, Wu L, Yan Y. Influence of formic acid on corrosion behavior of bronze under thin Electrolyte Layer. J Wuhan Univ Technology-Mater Sci Ed. 2022;37:482–9.
37. Yan Y, Zou C, Zhang L, Zhu Y, Wu L, Zhou H. Cai L. A study on Corrosion products and processes of patinated tin bronze in formic acid. Res Chem Intermed. 2020;46:5087–99.
38. Sheikhi S, Jalali F. Hierarchical $Nico_2o_4$/Cuo-C nanocomposite derived from copper-based metal Organic Framework and Ni/Co Hydroxides: excellent electrocatalytic activity towards methanol oxidation. J Alloys Compd. 2022;907:164510.
39. Ma W, Zhang S, Chen Y, Zhong D, Du Q, Li J, Li R, Du X, Zhang J, Yu T. Fe_3o_4-Cuo@Lignite activated Coke activated Persulfate Advanced Treatment of Phenolic Wastewater from Coal Chemical Industry. Environ Res. 2022;213:113601.
40. Uma HB, Kumar MSV, Ananda S. Semiconductor-Assisted photodegradation of Textile Dye, Photo-Voltaic and Antibacterial Property of Electrochemically Synthesized Sr-Doped Cuo Nano Photocatalysts. J Mol Struct. 2022;1264:133110.
41. Dhilip Kumar R, Sreevani K, Radhika G, Sethuraman V, Shanmugavalli V, Nagarani S, Balachandran S, Kumar M. One-Pot synthesis of Cuo-Cu_2o nanoscrubbers for high-performance pseudo-supercapacitors applications. Mater Sci Eng: B. 2022;281:115755.

Publisher's Note